Title

Hybridization and deconfinement in colloidal quantum dot molecules

Journal

The Journal of Chemical Physics, 157(13)

ISSN

0021-9606

Authors

Verbitsky, Lior
Jasrasaria, Dipti
Banin, Uri
et al.

Publication Date

2022-10-07

DOI

10.1063/5.0112443

Peer reviewed

The Journal of Chemical Physics

RESEARCH ARTICLE | OCTOBER 07 2022

Hybridization and deconfinement in colloidal quantum dot molecules

Special Collection: 40 Years of Colloidal Nanocrystals in JCP

Lior Verbitsky ; Dipti Jasrasaria ; Uri Banin ; Eran Rabani

J. Chem. Phys. 157, 134502 (2022)
https://doi.org/10.1063/5.0112443
CHORUS

The Journal of Chemical Physics ARTICLE scitation.org/journal/jcp

Hybridization and deconfinement in colloidal quantum dot molecules

Cite as: J. Chem. Phys. 157, 134502 (2022); doi: 10.1063/5.0112443
Submitted: 21 July 2022 • Accepted: 9 September 2022 •
Published Online: 7 October 2022

Lior Verbitsky,[1,a] Dipti Jasrasaria,[2,b] Uri Banin,[1,c] and Eran Rabani[2,3,4,d]

AFFILIATIONS

[1] The Institute of Chemistry and The Center for Nanoscience and Nanotechnology, The Hebrew University of Jerusalem, Jerusalem 9190401, Israel
[2] Department of Chemistry, University of California, Berkeley, California 94720, USA
[3] The Sackler Center for Computational Molecular and Materials Science, Tel Aviv University, Tel Aviv, 69978, Israel
[4] Materials Sciences Division, Lawrence Berkeley National Laboratory, Berkeley, California 94720, USA

Note: This paper is part of the JCP Special Topic on 40 Years of Colloidal Nanocrystals in JCP.
[a] lior.verbitsky@mail.huji.ac.il
[b] djasrasaria@berkeley.edu
[c] **Electronic mail:** uri.banin@mail.huji.ac.il
[d] **Author to whom correspondence should be addressed:** eran.rabani@berkeley.edu

ABSTRACT

The structural, electronic, and optical properties of CdSe/CdS core–shell colloidal quantum dot molecules, a new class of coupled quantum dot dimers, are explored using atomistic approaches. Unlike the case of dimers grown by molecular beam epitaxy, simulated strain profile maps of free-standing colloidal dimers show negligible additional strain resulting from the attachment. The electronic properties of the relaxed dimers are described within a semiempirical pseudopotential model combined with the Bethe–Salpeter equation within the static screening approximation to account for electron–hole correlations. The interplay of strain, hybridization (tunneling splitting), quantum confinement, and electron–hole binding energies on the optical properties is analyzed and discussed. The effects of the dimensions of the neck connecting the two quantum dot building blocks, as well as the shell thickness, are studied.

INTRODUCTION

Colloidal quantum dots (CQDs), also known as "artificial" atoms,[1–5] have become robust emitters with tunable optoelectronic properties, which are controlled by their size and composition.[6–8] Recently, coupled CQD molecules (CQDM) were synthesized via the fusion of two core–shell CQDs, manifesting signatures of "artificial" molecules showing spectral shifts, spectral broadening, and lifetime shortening, observed by ensemble and single molecule measurements.[9–12] The presence of two coupled emission centers in a single quantum system as well as other unique attributes of CQDM opens the door to exploring the electronic and optical properties in regimes that were previously inaccessible. Particularly, the design and the positioning of the two emission centers offers an additional knob to control many-body interactions in the form of multiple (neutral and charged) excitations.[13,14]

Tailoring the optoelectronic functionalities of CQDM requires a deep understanding of their electronic and optical characteristics as well as the dependence of these characteristics on the size of the CQD building blocks, the separation between their centers, the attachment orientation of the two CQDs and on the nature of the connecting interfacial area between the two emitting centers, the so called "neck," which defines the tunneling barrier and can be modified by varying its girth. Some of these issues were recently addressed using the effective mass approximation,[6,10,11,15] which lacks an atomistic description necessary to account for the orientation of attachment, as well as strain and stress effects.

In this work, we performed atomistic calculations to determine the structure and electronic properties of CQDM composed of two fused CdSe/CdS core–shell CQDs as a model system. The configurations of all the CQDMs were optimized using mechanical force-fields,[16,17] and the corresponding electronic and optical properties were described within the semiempirical pseudo-potential model[18] combined with a nonperturbative description of electron–hole correlations [Bethe-Salpeter Equation (BSE)].[19] The calculations and theoretical analysis allow us to delineate the roles of confinement,

hybridization, and strain in different planes of attachment while varying the shell thickness and neck girth. The modifications of the electronic properties in the CQDMs are attributed to a combination of factors, including hybridization energies, loss of confinement in the presence of a neck (which we hereon refer to as "deconfinement"), and modified electron–hole interactions. Strong excitonic redshifts are predicted for dimers composed of fully fused quantum dots (QDs) with a thin shell. The work sets an atomistic theoretical framework to also predict further optoelectronic characteristics of colloidal quantum dots. Interestingly, we also find that the quasi-hole comprising the lowest exciton changes symmetry with the orientation of attachment. A related effect of the quasi-hole was reported for InAs/GaAs dimers grown by molecular beam epitaxy,[20–23] where the symmetry of the hole was correlated with the distance between the two InAs/GaAs quantum dots. Moreover, comparing the postdictions of our model to the experimental measurements, we find excellent agreement in describing the overall spectral red shifts in photoluminescence (PL) and in the absorption as well as spectral broadening and changes in oscillator strengths.

RESULTS AND DISCUSSION

We considered three sizes of core–shell CdSe/CdS QDs with a D_{core} = 2.8 nm core diameter and varying shell thicknesses, with a total diameters ranging from D = 4.6 nm to D = 7 nm, as illustrated in Fig. 1. The QDs can be attached in either[10] the [100] or the [001] orientations and additional layers of CdS can be added to the neck area to control its width. The configurations of all the CQDMs used in the study were optimized using mechanical force fields[16] implemented within Large-scale Atomic/Molecular Massively Parallel Simulator (LAMMPS).[17] The nanostructure construction process is described schematically in Fig. S1 and in detail in the supplementary material, with the full list of nanostructure configurations in Table S1.

In Fig. 1, we plot the strain profile of a CdSe/CdS core–shell QD and compare it to the strain profile of two attached dimers. These strain profiles were generated by relaxing the stress generated by the growth of a CdS shell on the CdSe core as well as the stress resulting from the attachment of the two monomers, and are in agreement with previously documented strain patterns and magnitudes.[24,25] The relatively large compressive strain of the CdSe core atoms has been reported previously and was used to rationalize the behavior of pressure-induced structural transformation with varying shell thickness.[26] We find that the attachment of the two QDs results in negligible additional strain on the CdSe core atoms or on the CdS shell atoms regardless of the plane of attachment. Furthermore, the absence of strain (and stress) in the neck region is apparent, as expected for defect-less attachments.[27,28]

Typical solutions for the quasi-electron wavefunctions for the ground and first excited states are shown in Fig. 2. The quasi-electron ground and first excited orbitals can roughly be described by a symmetric and asymmetric superposition of the $1S_e$-like envelope functions of the QD monomer building blocks. The hybridization energy of the electron (Δ_e, sometime referred to as the "tunneling splitting") can then be approximated by half the energy difference between the two lowest quasi-electron states, $\Delta_e = \frac{1}{2}(E_{e_2} - E_{e_1})$. Similarly, the quasi-hole tunneling splitting is given by $\Delta_h = \frac{1}{2}(E_{h_1} - E_{h_2})$. Together, both effects are expected to change the overall fundamental gap by $\Delta_g = (\Delta_h + \Delta_e)$. However, since the quasi-hole has a relatively heavy effective mass and experiences a large band offset at the core/shell interface, it remains localized to the CdSe core regions (and not the CdS shell), resulting in negligibly small hybridization energies ($\Delta_h \ll 1$ meV). Therefore, the main contribution to the changes in the fundamental gap due to hybridization can be assigned to the quasi-electron ($\Delta_g \approx \Delta_e$), which is shown in the lower right panel of Fig. 2. In the lower

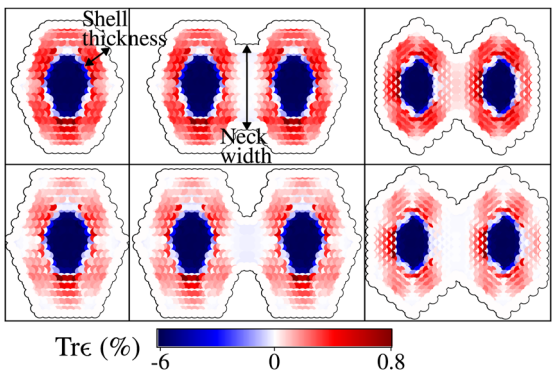

FIG. 1. Color-coded strain profiles of a D = 4.6 nm (upper panels) and D = 7 nm (lower panels) CdSe/CdS core–shell monomer (left panels), and of two CQDMs attached along the planes [100] with ≈3 and ≈2 nm neck widths, respectively, (middle panels) and [001] with ≈3 and ≈3.5 nm neck widths, respectively (right panels). Black outlines are the location of the passivating pseudo-atoms.

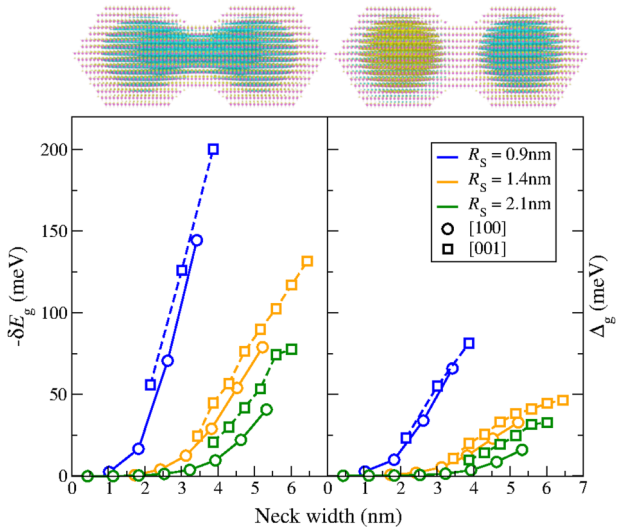

FIG. 2. Upper panels: Hyper-sphere plots of the quasi-electron lowest (left panel) and first excited (right panel) wavefunctions (yellow and turquoise denoting opposite signs) of D = 5.6 nm dimers attached through the [100] axis with a ≈4 nm neck and $\Delta_g \approx 20$ meV. Lower panels: The shift in the fundamental gaps, δE_g (left panel), and the tunneling splitting, Δ_g (right panel), as a function of neck width for QDs with D = 4.6 nm (blue symbols), D = 5.6 nm (orange symbols), and D = 7 nm (green symbols). Circles (squares) connected by solid (dashed) line corresponds to the [100] ([001]) plane of attachments.

left panel of Fig. 2, we plot the overall change in the fundamental gap ($\delta E_g = \delta E_e - \delta E_h \approx \delta E_e$, where $\delta E_{e/h}$ are the changes in the quasi-electron/hole energies in the CQDMs relative to the monomer CQD) as a function of the neck width for all dimers studied in this work. We find that below an onset width of about ≈2 nm, namely, for neck widths that are smaller than the size of the CdSe core, the changes in δE_g and Δ_g are rather small. As the neck grows beyond ≈2 nm, Δ_g increases and slowly approach a plateau while $|\delta E_g|$ continually increases across all neck sizes studied. The dependence on the shell thickness is mainly governed by changes in the core-to-core distance mitigated by changes in the confinement energy of the quasi-electron as the shell thickness is varied. We also find slightly larger shifts for the [001] orientation attachment resulting from shorter core-to-core distances.

Perhaps somewhat surprising is the large difference between the calculated shifts for $|\delta E_g|$ and for Δ_g, suggesting that the renormalization of the fundamental gap is not solely governed by the strength of hybridization, which has been assumed in many previous studies.[9–11,20,21,29,30] To better understand this difference observed between δE_g and Δ_g, we express the overall shift in the quasiparticle gap as a sum of three contributions,

$$\delta E_g = -\Delta_g + \delta E_q + \delta E_s, \tag{1}$$

where δE_q and δE_s account for the change in the quasiparticle gap resulting from changes in the quantum confinement and strain energies, respectively. To delineate the role of the neck, we compare the fundamental gaps computed for a single QD with that of a QD with just the neck attached (referred to as "deconfined" QD), as illustrated in Fig. 3(a). The deconfined structure accounts for both δE_q and δE_s but since the structure is comprised of only one QD, $\Delta_g = 0$. We find that the changes in δE_g resulting from changes in the strain of the attachment QD monomers are rather small ($\delta E_s < 1$ meV), specifically $\delta E_s \ll \delta E_q$, and thus can be ignored to a first approximation. Strain may become important for hetero-structures with larger lattice mismatch.[20–22] A comparison of the shifts computed for the QD dimer, δE_g, and the contributions from hybridization and confinement energies, $-\Delta_g + \delta E_q$, is shown in Fig. 3(b). We find that the two calculations agree with each other to within ≈10% for a wide range of neck thicknesses, indicating that a significant (≈50%) change of the quasiparticle gap results from a decrease in the confinement energy of the electron–hole pair in the presence of a neck. This is the case also for other shell thicknesses, as shown in Fig. S2 for $D = 4.6$ nm.

In Figs. 3(c) and 3(d), we compare the energy shifts of the two lowest quasi-electron states [panel (c)] and that of the highest quasi-hole state [panel (d)] as the neck width is varied. The changes in the quasi-hole energy are rather small (≈ ±1 meV) and are difficult to converge numerically due to limitations of the approach because of the high density of hole states at the valence band edge. The changes in the quasi-electron energies are significantly larger compared to the quasi-hole energies, and may exceed 50 meV for thick necks. Comparing the changes in the lowest quasi-electron energy (orange symbols) to the first excited state (green symbols), we find that they are not symmetric as expected for a two-state model, signifying the role of higher monomer excitations ($1P_e$, $2S_e$, etc.) that mix to form the symmetric and asymmetric quasi-electron states.

So far, we focused on single-particle properties, however, to make connections with optical measurements, we need to account for electron–hole correlations. Perturbation techniques are useful when the exciton binding energy is much smaller than all the other energy scales (i.e., for strongly confined QDs), which is not the case of QD dimers, where the exciton binding energies are comparable to the hybridization energies. Thus, to properly account for electron–hole correlations, we use the Bethe–Salpeter equation[14,19] within the static screening approximation (described by setting a constant, uniform, dielectric constant $\varepsilon = 6$) to calculate the

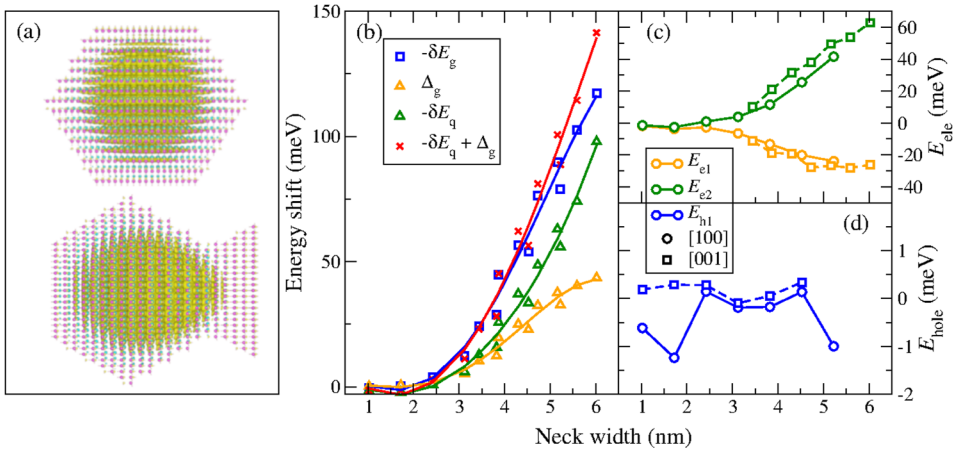

FIG. 3. (a) Hyper-sphere plots of the quasi-electron ground state wave functions for a core–shell CdSe/CdS QD ($D = 5.6$ nm) and a "deconfined" QD with an additional ≈3 nm neck. (b) The shift of the fundamental gap δE_g for QDs with $D = 5.6$ nm, comparing the full calculation (blue circles) to shift due to deconfinement δE_q (green triangles), due to hybridization Δ_g (orange squares) and their sum (red crosses). The lines are a guide for the eye. (c) and (d) Shifts of the two lowest quasi-electron energies (E_{e_1} (orange), E_{e_2} (green), and E_{h_1} (blue) energies) in [100] (circles connected by solid lines) and [001] (squares connected by dashed lines) relative to the corresponding energies calculated for the "deconfined" structures.

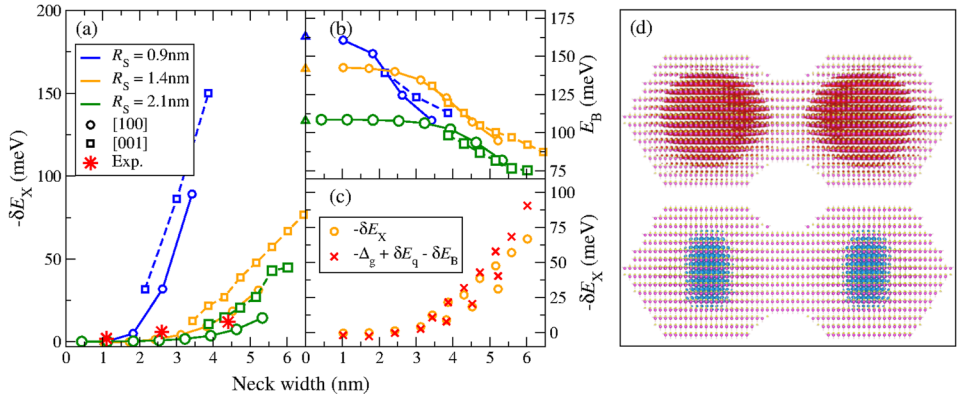

FIG. 4. (a) The shift in the optical gaps, δE_X, and (b) the shift in the exciton binding energy, E_B, as function of neck width for QDs with a total diameter D = 4.6 nm (blue symbols), D = 5.6 nm (orange symbols), and D = 7 nm (green symbols). Circles (squares) connected by solid (dashed) line correspond to the [100] ([001]) plane of attachment. Experimental shifts in the optical gaps of D = 7 nm QDs (red asterisks) are included for comparison.[11] (c) The shift of the optical gaps (orange symbols), for the D = 5.6 nm series of dimers compared to Eq. (2) (red crosses). (d) Hyper-sphere plots of hole (blue) and electron (red) densities projected from the excitonic wave function of D = 5.6 nm dimers attached through the [100] axis with a ≈3 nm neck.

excitonic states using the single-particle states found earlier as a basis. Other methods, such as configuration-interaction expansions[31] can be used as well to account for electron–hole interactions. More details on the application of the BSE in this work can be found in the supplementary material.

The behavior of the optical gaps is qualitatively similar to that of the fundamental gaps, as shown in Fig. 4(b). The predicted energy shifts for the D = 7 nm (green symbols, [001] attachment) are compared to the experimental results of Ref. 11 (red symbols), showing a very reasonable agreement. The dependence of the exciton binding energy, $E_B = E_g - E_X$, on the neck width is shown in Fig. 4(b). We find that above shell thickness larger than the core size (namely, above 2 nm for the present study), the exciton binding energy decreases with the neck width, consistent with the increase in the volume as the neck grows. Using the connection $E_g = E_X + E_B$ and the approximation in Eq. (1) (for $\delta E_s \approx 0$), one can show that $(\delta E_g = \delta E_X + \delta E_B = -\Delta_g + \delta E_q)$,

$$\delta E_X = \delta E_g - \delta E_B \approx -\Delta_g + \delta E_q - \delta E_B. \quad (2)$$

In Fig. 4(c), we compare the results predicted by the above expression with the calculated values for δE_X. As the neck width increases, we find a systematic deviation between the two, reminiscent of the deviation observed for δE_g in Fig. 3(b). Assuming that the change in the exciton binding energy can be expressed as $\delta E_X \approx -\Delta_X + \delta E_{Xc}$ (δE_{Xq} is the change in the exciton energy resulting from changes in the confinement), we find that the reduction in the confinement energy of the excitons is responsible for >80% of the observed shift in the optical gap compared to only 50% for the fundamental gap (see Fig. S3). This difference in behavior results from the localization of the excitons to the QD cores [see Fig. 4(d)] due to the localized nature of the quasi-holes compared to the free quasi-electron, thereby reducing the hybridization of the electrons. Thus, in the case of quasi-type-II systems such as CdSe/CdS the observed experimental optical shifts are mainly affected by the reduction of confinement energy rather than strong excitonic hybridization.

In the top panels of Fig. 5, we plot the direction-averaged absorption cross section at the onset of absorption for various neck widths (color coded). We find that for the narrowest neck studied, the peak absorption is nearly twice as high compared to the corresponding transition in the monomer. As the neck width increases by adding more layers of CdS to the neck area, the absorption peak intensity decreases and widens, approaching gradually the peak

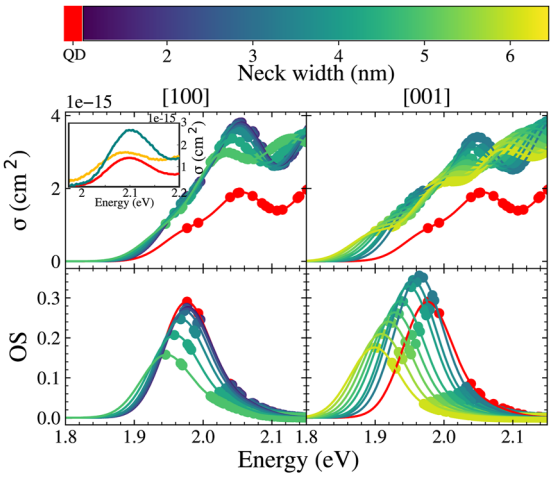

FIG. 5. Upper panels: Calculated absorption spectra in [100]-attached (upper left panel) [001]-attached (upper right panel) QD dimers with a diameter of D = 4.6 nm as function of neck width (color coded) compared to the original QD spectrum (red). Dots indicate the position of the excitonic eigenstates. The inset in the upper left panel shows experimental results for the absorption cross section for a QD (red), a dimer bound by a linker (no neck, green), and a fused QD dimer (yellow).[15] Bottom panels: The corresponding calculated oscillator strengths (OS) for emission.

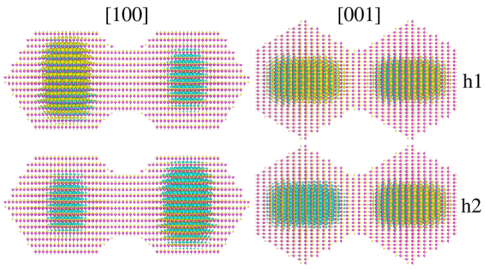

FIG. 6. The two highest-in-energy single-particle hole states in a [100] (left panels) and [001] (right panels) dimers of $D = 4.6$ nm QDs a with a ≈3 nm neck.

height of the QD building blocks. The inset in the upper left panel of Fig. 5 shows quantitatively similar results observed experimentally for CdSe/CdS CQDMs,[10,11] further validating the model and the computational framework, and confirming that the experimentally observed reduction in the absorption peak intensity with increasing neck width is a result of reduction in oscillator strength and therefore is an intrinsic property.

In the bottom panels of Fig. 5, we plot the emission spectra of the QD dimers attached along the [100] axis and [001] axis. The former attachment shows a monotonic decrease in the oscillator strength (OS) with increasing neck width while for the latter attachment, the OS first increases by ≈30%, followed by a decrease with increasing neck width. The difference between the two orientations can be explained by comparing the quasi-hole (single-particle) ground and first excited state for each orientation (Fig. 6). The quasi-hole ground state envelope function along the [001] attachment is positive while that along the [100] attachment changes sign, rendering the lowest-in-energy transitions dipole-forbidden. This also explains the difference between the absorption cross sections of the two attachment orientations, shown in Fig. 5. Similar behavior was predicted[20–22] and experimentally validated[23] for InAs/GaAs dimers grown by molecular beam epitaxy. While orientation dependence was not studied in those cases, it was found that the symmetry of the hole ground state flips from symmetric to anti-symmetric at a critical distance, owing to the dominant hybridized hole state (p-like vs s-like). The theoretical analyses used the spin–orbit interaction of the hole states, for example by contrasting four-band $k \cdot p$ models with single-band effective-mass models, in order to explain this distance-dependent reversal. Interestingly, our model neglects the spin–orbit interaction and yet predicts a similar effect by merely implicitly introducing orientation-dependent hybridization of hole states that effectively leads to a flip in the tunneling matrix element sign.

CONCLUSIONS

The structural, electronic, and optical properties of colloidal quantum dot molecules were studied using mechanical force fields, atomistic pseudopotential models combined with the Bethe–Salpeter equation, providing important insights on the role of strain, stress, hybridization, deconfinement, and exciton binding energies of CQDMs. We find that the quasi-particle gap red-shifts upon fusion into the CQDM relative to the monomers, and the shift increases significantly upon neck-filling for neck widths larger than the size of the QD building blocks. As expected, the quasi-electron shifts dominate the behavior, with a significant contribution resulting from deconfinement combined with contribution of the quasi-electron hybridization energy. Strain effects are negligible in the free standing CQDM system, unlike the behavior of self-assembled MBE grown quantum dot molecules. Moreover, the fusion orientation is not a major factor in dictating the energetics for the studied cases. Taking into account electron–hole correlation, we find that the optical gap shifts calculated within the Bethe–Salpeter approach are in good agreement with the experimental data, and the magnitude of the shifts is governed by the strength of hybridization and deconfinement of the excitons, as well as changes in the exciton binding energy upon fusion. The calculated absorption spectra of the CQDM show qualitative agreement with the experiments, specifically, a red shift and broadening at the gap, and doubling of the oscillator strength at high energies.

The developed methodology thus provides a powerful theoretical framework for addressing further coupling and interaction mechanisms in CQDMs. For example, the binding energies and decay rates of biexcitons and other multiexcitonic states. Similar methodology can be applied to CQDMs of other compositions, which could manifest diverse behaviors depending on the system parameters as they arise from the respective band structure. 40 years after the birth of colloidal quantum dots, we progress to artificial QD molecules, an important development that expands the research landscape and possible functionalities of colloidal quantum dots based systems.

SUPPLEMENTARY MATERIAL

See the supplementary material for computational methods and additional figures noted in the main text.

ACKNOWLEDGMENTS

This work was supported by the NSF–BSF International Collaboration in the Division of Materials Research Program (NSF Grant No. DMR-2026741 and BSF Grant No. 2020618). Methods used in this work were provided by the Center for Computational Study of Excited State Phenomena in Energy Materials (C2SEPEM), which is funded by the U.S. Department of Energy, Office of Science, Basic Energy Sciences, Materials Sciences and Engineering Division, via Contract No. DE-AC02- 05CH11231, as part of the Computational Materials Sciences Program. Computational resources were provided, in part, by the National Energy Research Scientific Computing Center (NERSC), a U.S. Department of Energy Office of Science User Facility operated under Contract No. DE-AC02-05CH11231. U.B. thanks the Alfred & Erica Larisch memorial chair. D.J. acknowledges the support of the Computational Science Graduate Fellowship from the U.S. Department of Energy under Grant No. DE-SC0019323.

AUTHOR DECLARATIONS

Conflict of Interest

The authors have no conflicts to disclose.

Author Contributions

Lior Verbitsky: Conceptualization (equal); Data curation (equal); Formal analysis (equal); Investigation (equal); Visualization (equal); Writing – original draft (equal). **Dipti Jasrasaria**: Formal analysis (supporting); Investigation (supporting); Methodology (supporting); Writing – review & editing (supporting). **Uri Banin**: Conceptualization (equal); Formal analysis (equal); Funding acquisition (equal); Project administration (equal); Resources (equal); Supervision (equal); Writing – review & editing (equal). **Eran Rabani**: Conceptualization (equal); Formal analysis (equal); Funding acquisition (equal); Methodology (equal); Project administration (equal); Resources (equal); Supervision (equal); Writing – review & editing (equal).

DATA AVAILABILITY

The data that support the findings of this study are available within the article and its supplementary material.

REFERENCES

[1] L. E. Brus, J. Chem. Phys. **80**, 4403 (1984).
[2] A. I. Ekimov, A. L. Efros, and A. A. Onushchenko, Solid State Commun. **56**, 921 (1985).
[3] A. P. Alivisatos, Science **271**, 933 (1996).
[4] U. Banin, Y. Cao, D. Katz, and O. Millo, Nature **400**, 542 (1999).
[5] C. L. Choi and A. P. Alivisatos, Annu. Rev. Phys. Chem. **61**, 369 (2010).
[6] Y. E. Panfil, M. Oded, and U. Banin, Angew. Chem., Int. Ed. **57**, 4274 (2018).
[7] C. R. Kagan, L. C. Bassett, C. B. Murray, and S. M. Thompson, Chem. Rev. **121**, 3186 (2020).
[8] F. P. G. de Arquer, D. V. Talapin, V. I. Klimov, Y. Arakawa, M. Bayer, and E. H. Sargent, Science **373**, eaaz8541 (2021).
[9] B. K. Hughes, J. L. Blackburn, D. Kroupa, A. Shabaev, S. C. Erwin, A. L. Efros, A. J. Nozik, J. M. Luther, and M. C. Beard, J. Am. Chem. Soc. **136**, 4670 (2014).
[10] J. Cui, Y. E. Panfil, S. Koley, D. Shamalia, N. Waiskopf, S. Remennik, I. Popov, M. Oded, and U. Banin, Nat. Commun. **10**, 5401 (2019).
[11] J. Cui, S. Koley, Y. E. Panfil, A. Levi, Y. Ossia, N. Waiskopf, S. Remennik, M. Oded, and U. Banin, J. Am. Chem. Soc. **143**, 19816 (2021).
[12] S. Koley, J. Cui, Y. E. Panfil, and U. Banin, Acc. Chem. Res. **54**, 1178 (2021).
[13] Y. E. Panfil, J. Cui, S. Koley, and U. Banin, ACS Nano **16**, 5566 (2022).
[14] D. Jasrasaria, D. Weinberg, J. P. Philbin, and E. Rabani, J. Chem. Phys. **157**, 020901 (2022).
[15] Y. E. Panfil, D. Shamalia, J. Cui, S. Koley, and U. Banin, J. Chem. Phys. **151**, 224501 (2019).
[16] X. W. Zhou, D. K. Ward, J. E. Martin, F. B. van Swol, J. L. Cruz-Campa, and D. Zubia, Phys. Rev. B **88**, 085309 (2013).
[17] A. P. Thompson, H. M. Aktulga, R. Berger, D. S. Bolintineanu, W. M. Brown, P. S. Crozier, P. J. in't Veld, A. Kohlmeyer, S. G. Moore, T. D. Nguyen, R. Shan, M. J. Stevens, J. Tranchida, C. Trott, and S. J. Plimpton, Comput. Phys. Commun. **271**, 108171 (2022).
[18] E. Rabani, B. Hetényi, B. J. Berne, and L. E. Brus, J. Chem. Phys. **110**, 5355 (1999).
[19] M. Rohlfing and S. G. Louie, Phys. Rev. B **62**, 4927 (2000).
[20] G. Bester, A. Zunger, and J. Shumway, Phys. Rev. B **71**, 075325 (2005).
[21] W. Jaskólski, M. Zieliński, G. W. Bryant, and J. Aizpurua, Phys. Rev. B **74**, 195339 (2006).
[22] J. I. Climente, M. Korkusinski, G. Goldoni, and P. Hawrylak, Phys. Rev. B **78**, 115323 (2008).
[23] M. F. Doty, J. I. Climente, M. Korkusinski, M. Scheibner, A. S. Bracker, P. Hawrylak, and D. Gammon, Phys. Rev. Lett. **102**, 047401 (2009).
[24] K. Gong, G. Beane, and D. F. Kelley, Chem. Phys. **471**, 18 (2016).
[25] S.-H. Lohmann, P. Harder, F. Bourier, C. Strelow, A. Mews, and T. Kipp, J. Phys. Chem. C **123**, 5099 (2019).
[26] M. Grünwald, K. Lutker, A. P. Alivisatos, E. Rabani, and P. L. Geissler, Nano Lett. **13**, 1367 (2012).
[27] J. C. Ondry, J. P. Philbin, M. Lostica, E. Rabani, and A. P. Alivisatos, ACS Nano **13**, 12322 (2019).
[28] J. C. Ondry, J. P. Philbin, M. Lostica, E. Rabani, and A. P. Alivisatos, ACS Nano **15**, 2251 (2020).
[29] M. Bayer, P. Hawrylak, K. Hinzer, S. Fafard, M. Korkusinski, Z. R. Wasilewski, O. Stern, and A. Forchel, Science **291**, 451 (2001).
[30] J. Cassidy, M. Yang, D. Harankahage, D. Porotnikov, P. Moroz, N. Razgoniaeva, C. Ellison, J. Bettinger, S. Ehsan, J. Sanchez, J. Madry, D. Khon, and M. Zamkov, Nano Lett. **21**, 7339 (2021).
[31] A. Franceschetti, H. Fu, L. W. Wang, and A. Zunger, Phys. Rev. B **60**, 1819 (1999).